Inorg. Chem. **2005**, *44*, 2414–2425

Synthesis, Characterization, Physicochemical, and Photophysical Studies of Redox Switchable NIR Dye Derived from a Ruthenium–Dioxolene–Porphyrin System

D. Amilan Jose, Atindra D. Shukla, D. Krishna Kumar, Bishwajit Ganguly, and Amitava Das*

Central Salt and Marine Chemicals Research Institute, Bhavnagar 364 002, Gujarat, India

G. Ramakrishna, Dipak K. Palit, and Hirendra N. Ghosh*

Radiation Chemistry and Chemical Dynamics Division, Bhabha Atomic Research Center, Mumbai 400 085, India

Received August 29, 2004

Newly synthesized semi-quinone derivatives of the ruthenium polypyridyl, covalently linked to a porphyrin core, show very high ϵ values (59 000–83 500 $M^{-1}cm^{-1}$) for the absorption band in the near infrared (NIR) region of the spectrum. Further, complexes **1**–**4** show an interesting reversible electrochromic behavior as a function of the redox state of the coordinated dioxolene functionality, and a switching phenomenon between bleaching and the restoration of the NIR peak could be achieved electrochemically. Thus, complexes **1**–**4** could be ideal candidate materials for NIR-active electrochromic devices. Ultrafast studies on **1** and its mononuclear components, 5-(3,4-dihydroxyphenyl)-10,15,20-triphenyl-21H,23H-porphyrin (H_2L_1) and $Ru(bpy)_2(bsq)^+$, reveal that there is no electron or energy transfer from the porphyrin to the $Ru(bpy)_2sq^+$ (bpy is 2,2′-bipyridine and sq is the deprotonated species of a substituted semi-quinone fragment) fragment or vice versa in **1**. The observed decrease in the luminescence quantum yield for **1** compared to that of H_2L_1 can be ascribed to the increased nonradiative pathway due to higher vibronic coupling because of the direct linkage of the metal center to the porphyrin moiety.

Introduction

Molecular systems that absorb strongly in the near infrared (NIR) region are of considerable interest to both chemists and material scientists because of their potential in diverse applications such as optical data processing, photodynamic therapy, telecommunications, aerospace, military camouflage, and so forth.[1,2] Compounds that generally show strong absorption in the NIR region include Ni^{II}−dithiolene complexes, some mixed valence complexes, molecules with extended conjugated systems, and some conducting polymers.[2−6] However, studies in this area mostly involve discrete NIR-active molecules, and thus, the possibility to achieve on/off switching of the NIR absorption band as a function of the redox state of the chromophore is limited.[2,7−11] Lever

* Authors to whom correspondence should be sent. E-mail: amitava@csmcri.org (A.D.); hnghosh@magnum.barc.ernet.in (H.N.G.).

(1) (a) Emmelius, M.; Pawlowski, G.; Vollmann, H. W. *Angew. Chem., Int. Ed. Engl.* **1989**, *28*, 1445. (b) Sengupta, S.; Sadhukhan, S. K. *J. Chem. Soc., Perkin Trans. 1* **2000**, 4332. (c) Fabian, J.; Nakamura, I. L.; Matsuoka, M. *Chem. Rev.* **1992**, *92*, 1197. (d) Tsuda, A.; Osuka, A. *Science* **2001**, *293*, 79. (e) *Infrared Optical Circuits and Components: Design and Applications*; Murphy, E. J., Ed.; Marcel Dekker: New York, 1999. (f) Chandrasekhar, P.; Zay, B. J.; Birur, G. C.; Rawal, S.; Pierson, E. A.; Kauder, L.; Swanson, T. *Adv. Funct. Mater.* **2002**, *12*, 95.

(2) Ward, M. D.; McCleverty, J. A. *J. Chem. Soc., Dalton Trans.* **2002**, 275 and references therein.

(3) Mueller-Westerhof, U. T.; Vance, B.; Yoon, D. I. *Tetrahedron* **1991**, *47*, 909 and references therein.

(4) (a) Barthram, A. M.; Cleary, R. L.; Kowallick, R.; Ward, M. D. *Chem. Commun.* **1998**, 2695. (b) Cañadas, J. G.; Meacham, A. P.; Peter, L. M.; Ward, M. D. *Angew. Chem., Int. Ed.* **2003**, *42*, 3011.

(5) Blake, I. M.; Rees, L. H.; Claridge, T. D. W.; Anderson, H. L. *Angew. Chem., Int. Ed.* **2000**, *39*, 1818 and references therein.

(6) (a) Cho, H. S.; Jeong, D. H.; Cho, S.; Kim, D.; Matsuzaki, Y.; Tanaka, K.; Tsuda, A.; Osuka, A. *J. Am. Chem. Soc.* **2002**, *124*, 14643. (b) Shukla, A. D.; Bajaj, H. C.; Das, A. *Angew. Chem., Int. Ed.* **2001**, *40*, 446.

(7) (a) Mortimer, R. J. *Chem. Soc. Rev.* **1997**, *26*, 147. (b) Rosseinsky, D. R.; Mortimer, R. J. *Adv. Mater. (Weinheim, Ger.)* **2001**, *13*, 783.

(8) Haga, M.; Dodsworth, E. S.; Lever, A. B. P. *Inorg. Chem.* **1986**, *25*, 447.

(9) Lever, A. B. P.; Masui, H.; Metcalfe, R. A.; Stufkens, D. H.; Dodsworth, E. S.; Auburn, P. R. *Coord. Chem. Rev.* **1993**, *125*, 317.

(10) Schwab, P. F. H.; Diegoli, S.; Biancardo, M.; Bignozzi, C. A. *Inorg. Chem.* **2003**, *42*, 6613.

10.1021/ic048805l CCC: $30.25
Published on Web 03/05/2005

Chart 1

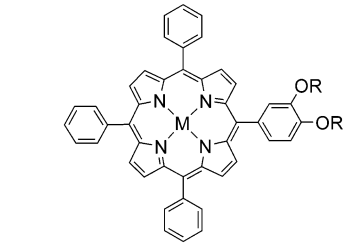

M = 2H, R = -CH_3; **Me_2L_1**
M = Zn, R = -CH_3; **Me_2L_2**
M = 2H; R = H; **H_2L_1**
M = Zn; R = H, **H_2L_2**

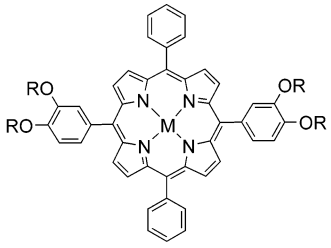

M = 2H, R = -CH_3; **Me_4L_3**
M = Zn, R = -CH_3; **Me_4L_4**
M = 2H; R = 4H; **H_4L_3**
M = Zn; R = 4H; **H_4L_4**

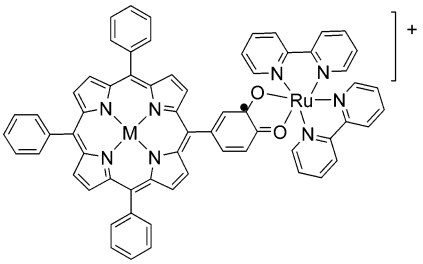

Complex **1** (M is 2H) and **2** (M is Zn(II))

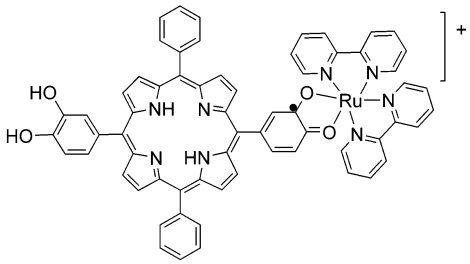

Complex **{(bpy)$_2$Ru(H_2L_3)$_{sq}$}$^+$**

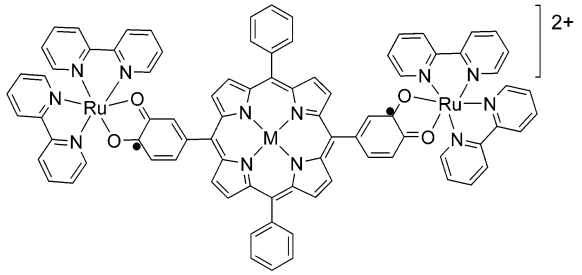

Complex **3** (M is 2H) and **4** (M is Zn(II))

and co-workers were the first[8] among different research groups[2,9−11] who could demonstrate that Ru(bpy)$_2$(bsq)$^+$ complexes (bpy is 2,2′-bipyridine and bsq is the deprotonated species of the benzo semi-quinone form of 1,2-dihydroxy-benzene) display an absorption band for the d$\pi_{Ru} \rightarrow \pi^*_{bsq}$ metal-to-ligand charge-transfer (MLCT) transition in the NIR region ($\epsilon_{890} = 9000$ dm^{3}mol^{-1}cm^{-1}), while their one-electron reduced [Ru(bpy)$_2$(cat); cat is the completely deprotonated form of 1,2-dihydroxy benzene] or oxidized [Ru(bpy)$_2$(q)$^{2+}$; q is its corresponding benzo quinone form] products do not have any significant absorption in that region. Since then, several molecules based on the Ru(bpy)$_2$(sq)$^+$ fragment (sq is deprotonated species of the substituted semi-quinone fragment) have been reported by various workers, which show very high ϵ values for the redox-active NIR band. Recently, with an attempt to develop efficient and realistic electrochromic devices, Ru(bpy)(sq)$^+$ molecules, with high ϵ values for the NIR absorption band, were anchored on nanocrystalline SnO_2 and showed reversible electrochromic behavior.[10] In both reports, researchers did not observe any photoinduced interfacial electron transfer between nanocrystalline semiconductor (SnO_2) particles and Ru(bpy)$_2$(bsq)$^+$ fragments. It is worth mentioning here that, apart from the reversible electrochromic behavior, a higher molar absorptivity value is also desirable to design an efficient and sensitive sensor device. There are only a few examples for inorganic metal complexes[2,14a] available in the literature[1d,2,6,14] that show exceptionally high molar absorptivity values for the absorption band in the NIR region; though, no redox

(11) (a) Shukla, A. D.; Das, A. *Polyhedron*, **2000**, *19*, 2605. (b) Ghosh, D.; Shukla, A. D.; Banerjee, R.; Das, A. *J. Chem. Soc. Dalton Trans*. **2001**, 1. (c) Shukla, A. D.; Whittle, B.; Bajaj, H. C. *Inorg. Chim. Acta* **1999**, *285*, 89.

(12) The thermodynamic driving force ($\Delta G°$) for the electron transfer process can be evaluated from the expression $\Delta G° = -E_{00} + [E^{ox(D)} - E^{red(A)}]$, while for the TPP, E_{00} is ~2.0 eV and the $[E^{ox(D)} - E^{red(A)}]$ value for TPP/TPP$^+$ (D) and Ru(bpy)$_2$sq/Ru(bpy)$_2$cat (A) couples is −0.16 eV. Thus, $\Delta G° > 1.8$ eV and is thermodynamically highly favorable.

(13) (a)Lee, S.-M.; Marcaccio, M.; McCleverty, J. A.; Ward, M. D. *Chem. Mater*. **1998**, *10*, 3271. (b) Yoshida, K.; Oga, N.; Kadota, M.; Ogasahara, Y.; Kubo, Y. *Chem. Commun.* **1992**, 1114. (c) Takahashi, K.; Gunji, A.; Yanagi, K.; Miki, M. *J. Org. Chem*. **1996**, *61*, 4784. (d) Coe, B. J.; Houbrechts, S.; Asselberghs, I.; Persoons, A. *Angew. Chem., Int. Ed.* **1999**, *38*, 366.

(14) (a) Fleischer, E. B.; Shachter, A. M. *Inorg. Chem.* **1991**, *30*, 3763. (b) Deviprasad, G. R.; Keshavan, B.; D'Souza, F. *J. Chem. Soc., Perkin Trans. 1* **1998**, 3133. (c) Shukla, A. D.; Ganguly, B.; Dave, P. C.; Samanta; A.; Das, A. *Chem. Commun.* **2002**, 2648.

switching for the NIR absorption band for these complexes was reported.[1d,2,5,13]

In our attempt to utilize the reversible on and off phenomena of this redox-active NIR band for developing redox as well as photoactive photochromic dye, we planned to couple this NIR-active $Ru(bpy)(sq)^+$ fragment to another redox or photoactive center that can interact with the former and induce a reversible bleaching of the NIR absorption band. Preliminary calculations for the thermodynamic feasibility of the photoinduced electron transfer from the donor porphyrin fragment to the acceptor $Ru(bpy)_2(bsq)^+$ unit (based on the ground-state redox potential values of the porphyrin and $Ru(bpy)_2(bsq)^+$ centers and the steady-state luminescence property for the porphyrin center[12]) reveal that it is possible to achieve photoinduced electron injection from the photoactive porphyrin center to the covalently linked $Ru(bpy)_2(sq)^+$ core. This, coupled with the possibility of achieving a fast charge recombination process in such a system, may make $Ru(bpy)_2(bsq)^+$ and porphyrin fragments ideal candidates for use in developing an efficient redox or photoactive photochromic dye. On the basis of available information, we have synthesized mono- and bis-dioxolene derivatives of porphyrin (Chart 1) for the syntheses of new complexes (**1**−**4**; Chart 1) derived from the $Ru(bpy)_2(sq)$ core with an attempt to develop a reversible redox/photoactive chromophoric dye. The dioxolene derivatives of porphyrin used in this study are either previously reported (H_2L_1) or newly synthesized (H_2L_2−H_2L_4) (Chart 1)[14a,b] and are used for the synthesis of complexes **1**−**4** (Chart 1). Part of the preliminary results were published in one of our earlier communications.[14c]

Experimental Section

I. Materials. H_2L_1,[14a,b] $Ru(bpy)_2Cl_2 \cdot 2H_2O$,[15] $Ru(bpy)_2(bsq)(PF_6)$,[8] and ferrocenium hexafluorophosphate ($FcPF_6$)[16] were prepared following known methods. $[Bu^t]_4NPF_6$ was used as a background electrolyte for the electrochemical studies and was recrystallized from an ethanolic solution before use. Diisopropylamine, pyridine, and acetonitrile were dried and distilled over CaH_2. Pyrrole was distilled under reduced pressure prior to use. All of the reactions were performed under an argon atmosphere unless stated otherwise. The water that was used was doubly distilled. All of the other chemicals and solvents were obtained locally and were used as such without further purification.

II. Physical Measurements. Microanalyses (C, H, and N) were performed using a Perkin−Elmer 4100 elemental analyzer. Electron-impact mass spectra were obtained on a Kratos MS9 instrument, and fast-atom bombardment (FAB) measurements were carried out on a VG-ZAB instrument, using 3-nitrobezyl alcohol as the matrix. Fourier transform infrared spectra were recorded as KBr pellets using a Perkin−Elmer Spectra GX 2000 spectrometer. Absorption spectra were recorded using a Shimadzu UV-3101 PC spectrophotometer. ^1H NMR spectra were recorded on a Bruker 200 MHz FT NMR (model: Avance-DPX 200), using $CDCl_3/CD_3CN$ as the solvent and tetramethylsilane as an internal standard. Electron paramagnetic resonance (EPR) spectra were recorded at room temperature and at 77 K on a Bruker ESP-300 spectrometer. Electrochemical experiments were performed on a CH-660A (USA) electrochemical instrument; a conventional three-electrode cell assembly was used. A saturated Ag/AgCl solution as a reference and platinum as the working electrode were used for all of the measurements. Ferrocene was added at the end of each experiment as an internal standard, and all of the potentials are quoted versus the ferrocene/ferrocenium (Fc/Fc^+) couple. Spectra of the electroreduced/-oxidized species were recorded either using a spectrophotometer (model: Shimadzu UV-3101 PC) under a dinitrogen atmosphere or by recording in situ spectra of the electroreduced/-oxidized species with a fiber-optic deep probe attached to an Ocean Optics 2000 CCD spectrophotometer. Room-temperature emission spectra were obtained using a Perkin−Elmer LS 50B luminescence spectrofluorimeter fitted with a red-sensitive photomultiplier. The fluorescence quantum yields (ϕ_f) were estimated in the appropriate solvents (as specified), using the integrated emission intensity of 5,10,15,20-tetraphenyl porphyrin (H_2TPP; $\phi_f = 0.11$ in benzene) and ZnTPP ($\phi_{f(S1)} = 0.033$) as a reference (eq 1)[17−19] for free base porphyrins and its metalated derivatives, respectively. The emission spectra recorded are not corrected, and hence, we rely on the relative differences in the quantum yields only.

$$\phi_f = \phi'_f (I_{sample}/I_{std})(A_{std}/A_{sample})(\eta^2{}_{sample}/\eta^2{}_{std}) \quad (1)$$

In eq 1, ϕ'_f is the absolute quantum yield for the porphyrin molecule used as a reference, I_{sample} and I_{std} are the integrated emission intensities, A_{sample} and A_{std} are the absorbances at the excitation wavelength, and $\eta^2{}_{sample}$ and $\eta^2{}_{std}$ are the respective refractive indices.

Femtosecond transient absorption measurements were carried out in a femtosecond tunable visible spectrometer, which has been developed on the basis of a multipass amplified femtosecond Ti: sapphire laser system from Avesta, Russia (1 kHz repetition rate at 800 nm, 50 fs, 800 μJ/pulse), and described earlier.[20] The 800 nm output pulse from the multipass amplifier is split into two parts to generate pump and probe pulses. One part, with 200 μJ/pulse, is frequency-doubled in BBO crystals to generate pump pulses at 400 nm. To generate visible probe pulses, about 3 μJ of the 800 nm beam is focused onto a 1.5-mm-thick sapphire window. The intensity of the 800 nm beam is adjusted by the iris size and neutral density filters to obtain a stable white-light continuum in the 400 nm to over 1000 nm region. The probe pulses are split into the signal and reference beams and are detected by two matched photodiodes with variable gains. We have kept the spot sizes of the pump and probe beams at the crossing point around 500 and 300 μm, respectively. The excitation energy density (at 400 nm) was adjusted to $\sim$2500 $\mu J/cm^2$. The noise level of the white light is about $\sim$0.5%, with occasional spikes that are due to oscillator fluctuation. We have noticed that most of the laser noise is low-frequency noise and can be eliminated by comparing the adjacent probe laser pulses (pump blocked vs unblocked, using a mechanical chopper). The typical noise in the measured absorbance change is about $<$0.3%. The instrument response function was obtained by fitting the rise time of the bleach of the sodium salt of *meso*-tetrakis-(4-sulfonatophenyl)porphyrin at 710 nm, which has an instantaneous response.

(15) Sullivan, B. P.; Salmon, D. J.; Meyer, T. J. *Inorg. Chem.* **1978**, *17*, 3334.
(16) (a) Decurtins, S.; Felix, F.; Ferguson, J.; Güdel, H. U.; Lud, A. *J. Am. Chem. Soc.* **1980**, *102*, 4102. (b) Connelly, N. G.; Geiger, W. E. *Chem. Rev.* **1996**, *96*, 877.
(17) Hill, R. L.; Gouterman, M.; Ulman, A. *Inorg. Chem.* **1982**, *21*, 1450.
(18) Ravikanth, M.; Chandrashekhar, T. K. *J. Photochem. Photobiol., A* **1993**, *74*, 181.
(19) Beeston, R. F.; Aldridge, W. S.; Treadway, J. A.; Fitzgerald, M. C.; DeGraff, B. A. E.; Stitzel, S. *Inorg. Chem.* **1998**, *37*, 4368.
(20) Ramakrishna, G.; Singh, A. K.; Palit, D. K.; Ghosh, H. N. *J. Phys. Chem. B.* **2004**, *108*, 1701.

Table 1. UV−Vis and Electrochemical Data of Ligands and Their Zn Derivatives

compound	λ_{max} ($CHCl_3$) ($\epsilon \times 10^4$ dm^3 mol^{-1} cm^{-1})	porphyrin-based $E_{1/2}$ (ΔE mV)[a]	dioxolene $E_{1/2}$ (ΔE mV)[a] sq/cat	dioxolene $E_{1/2}$ (ΔE mV)[a] sq/q
Me_2L_1	419 (298), 515 (15.5), 551(6.9), 591 (4.6), 647 (4.0)	0.81 (142), −1.73 (150) −2.06 (152)		0.5 (qr)
Me_2L_2	418 (301), 511 (2.6), 547 (19.6), 585 (3.4)	0.65 (100), −1.86 (100)		0.34 (qr)
H_2L_1	419 (283), 515 (13.8), 550 (5.7), 589 (4.0)	0.74 (100), −1.59 (100)		0.47 (ir)
H_2L_2	417 (308), 509 (5.5), 547 (37.5), 585 (6.1)	0.75 (100), −2.14 (120), −2.36 (120)		0.29[b] 0.47 (qr)
Me_4L_3	421 (252), 516 (10.9), 552 (6.0), 591 (3.4)	0.74, −1.72 (181), −2.05 (286)		0.47 (qr)
Me_4L_4	422 (283), 509 (2.2), 548 (16.2), 586 (3.2)	0.7 (100), −1.85 (100)		0.36 (qr)
H_4L_3[b]	420 (280), 516 (13.9), 552 (6.2), 591 (4.2)	1.2, 0.62, −1.23, −2.26	−0.34 (qr) −0.86(qr)	0.19, 0.35
H_4L_4[c]				

[a] Cyclic voltammograms were recorded in CH_2Cl_2 in 0.1 M $[Bu^t]_4NPF_6$. The potential values are reported (scan rate of 100 mV s^{-1}) versus those of the ferrocene/ferrocenium couple. Electrochemical measurements were made with Pt bead as the working electrode, Pt wire as the auxiliary electrode, and Ag−AgCl as the reference electrode. [b] Values are quoted from the square wave voltammogram. [c] Insoluble in common organic solvents.

The geometries of the model biradical (singlet and triplet forms) and quinonoid species were optimized following the unrestricted Hartree-Fock UHF method without any symmetry constraint by using the UPM3 Hamiltonian.[21,22]

III. Syntheses. A. H_2L_1. The synthesis of H_2L_1 was achieved following two different methodologies.

III.A.1. Method 1. The bis O-methylated product (Me_2L_1) was synthesized, as an intermediate, following a published procedure[14a,b] with some modifications in the purification process. Pyrrole (7 mL, 100mM), benzaldehyde (7.6 mL, 75 mM), and 3,4-dimethoxybenzaldehyde (4.1 g, 25 mM) were used for the reaction. The crude product was purified by column chromatography, using silica gel (60−120 mesh) as the stationary phase and $CHCl_3$/*n*-hexane (60:40 v/v) as the eluent. The desired product was isolated as a second fraction and was characterized by various analytical and spectroscopic techniques. Elem Anal. Calcd: C, 81.88; H, 5.04; N, 8.3. Found: C, 81.1; H, 5.1; N, 8.0. FAB−MS: 674 (M^+). ^1H NMR ($CDCl_3$, ppm): δ_H 8.91 (d, 2H, J = 4 Hz, $H_{pyrrole}$), 8.85 (d, 6H, J = 4 Hz, $H_{pyrrole}$), 8.22 (d, 6H, J = 8 Hz, H_{phenyl}), 7.78−7.71 (m, 11H, H_{phenyl}), 7.26 (d, 1H, J = 8.0 Hz, $H_{substituted\ phenyl}$), 4.18 (s, 3H, $H_{para-methoxy}$), 3.99 (s, 3H, $H_{meta-methoxy}$), −2.77 (s, 2H, H_{NH}). IR (KBr; ν/cm^{-1}): 3434 (−NH), 1026 (−OCH_3), 798−702 (pyrrole, HC═C). The desired product, H_2L_1, was obtained through demethylation from Me_2L_1 following the methodology reported earlier,[14a,b] except the reaction temperature was maintained at ∼160 °C. The final yield for H_2L_1 is 1.48 g (9.2%) with respect to the reactant pyrrole and different aldehydes used. Elem Anal. Calcd: C, 81.71; H, 4.68; N, 8.66. Found: C, 79.9; H, 4.3; N, 8.7. FAB−MS: 645 (M^+). ^1H NMR ($CDCl_3$, ppm): δ_H 8.82 (d, 8H, J = 4.8 Hz, $H_{pyrrole}$), 8.21 (d, 6H, J = 8.0 Hz, H_{phenyl}), 7.76−7.73 (m, 11H, H_{phenyl}), 7.58 (d, 1H, 8.0 Hz, $H_{substituted\ phenyl}$), −2.77 (s, 2H, H_{NH}). IR (KBr pellet; ν/cm^{-1}): 3448 (br, −NH and −OH), 1260 (C−O), 798 (pyrrole HC═C). UV−vis and $E_{1/2}$ values are summarized in Table 1.

III.A.2. Method 2. Benzaldehyde (7.6 mL, 75 mM) was dissolved in ∼200 mL of propionic acid in a two-neck round-bottom flask. 3,4-dihydroxybenzaldehyde (3.45 g, 25 mM) was added to this, the mixture was heated to ∼60 °C with vigorous stirring, and, then, freshly distilled and dry pyrrole (7.0 mL 100 mM) was added in a dropwise manner. The resulting mixture was allowed to reflux for 1 h. Then, the heat was removed, and the mixture was allowed to cool and was left overnight at room temperature. The solid was separated and removed by filtration, and it was found to be 5,10,15,20-tetraphenyl-21H,23H-porphyrin (H_2TPP). The filtrate was collected in a 500 mL conical flask and evaporated slowly on an oil bath, which yielded a dark-colored, sticky mass. This was washed with hot water to remove the remaining propionic acid and other undesired polymeric tars. Solid lumps obtained thereby were dried and subjected to gravity chromatography for purification; an ethyl acetate/methanol solvent mixture (97:3 v/v) as the eluent and silica gel as the stationary phase were used. This resulted in the desired product with a minor amount of H_2TPP as an impurity and was further purified by column chromatography on SiO_2, using ethyl acetate/*n*-hexane (80:20 v/v) as the eluent. The purified yield of the product was 1.1 g (∼6.8%). Analytical and various spectroscopic data are similar to those observed for H_2L_1 obtained by method 1.

III.B.1. Me_4L_3. Method 1. A total of 22.4 mL (0.32 M) of pyrrole was mixed with 0.8 mL (7.9 mM) of benzaldehyde. The mixture was degassed with argon for 30 min. Then, 0.068 mL of trifluoroacetic acid (TFA) was added slowly with a syringe strictly under an argon atmosphere while the color of the reaction mixture changed to dark orange-brown. About 15 mL of CH_2Cl_2 was added to this and was allowed to stir at room temperature for ∼45 min while the progress of the reaction was monitored by thin-layer chromatography (TLC). Then, the reaction mixture was diluted with ∼100 mL of CH_2Cl_2. The organic layer was washed with 0.1 N NaOH solution followed by distilled water. This organic layer was collected and dried over Na_2SO_4. After the removal of CH_2Cl_2, the unreacted pyrrole was removed from the concentrated mass at a pressure of ∼0 mbar and a temperature of 50−55 °C. The product, *meso*-phenyldipyrromethane, was identified as having a pale yellow color with R_f = 0.46 [on a silica gel TLC plate with $CHCl_3$/*n*-hexane/triethylamine (68:30:2 v/v/v) as the eluent]. For purification, this dark-yellow-colored, sticky mass was subjected to flash chromatography with 230−400 mesh-size silica gel and a cyclohexanes/ethyl acetate/triethylamine (79:20:1 v/v/v) mixture as the eluent. Yield: 1.25 g (∼70%). ^1H NMR ($CDCl_3$, ppm): δ_H 7.9 (br

(21) Reports on the calculations of porphyrin and its related isomers suggest that the UHF method seems to be a better choice than RHF for porphyrin systems. (Reynolds, C. H. *J. Org. Chem.* **1988**, *53*, 6061). Therefore, all of the geometries have been completely optimized without any symmetry constraints by using the UPM3 Hamiltonian.

(22) Stewart, J. J. P. *J. Comput. Chem.* **1989**, *10*, 209.

s, 2H, H_{NH}), 7.35−7.19 (m, 5H, H_{phenyl}), 6.7 (d, 2H, $H_{pyrrole}$), 6.17 (d, 2H, $H_{pyrrole}$), 5.9 (t, 2H, $H_{pyrrole}$), 5.48 (s, 1H, H_{meso-H}).

A total of 1.6 g (7.2 mM) of *meso*-phenyldipyrromethane and 1.2 g (7.2 mM) of 3,4-dimethoxybenzaldehyde were dissolved in ∼80 mL of degassed dichloromethane. The solution was stirred in an inert atmosphere for 30 min. To this, 2 to 3 drops of TFA were added as a catalyst. The mixture was stirred vigorously in the dark for 15 h, a 4 mol equiv of chloranil (∼7.0 g) was added, and the mixture was heated to reflux for 1 h. Then, it was cooled to room temperature and filtered. The filtrate was washed with 0.1N NaOH solution followed by distilled water to remove TFA. The organic layer was collected and dried. The desired product was purified by column chromatography, using silica gel (100−200 mesh) as the stationary phase and $CHCl_3$/*n*-hexane (80:20 v/v) as the eluent. The major purple fraction was found to contain the desired product. Yield: 0.200 g (∼7.5%). Elem Anal. Calcd: C, 78.47; H, 5.17; N, 7.62. Found: C, 78.6; H, 5.0; N, 7.5. FAB−MS: 734 (M^+). ^{1}H NMR ($CDCl_3$, ppm): δ_H 8.91 (d, 4H, J = 4.0 Hz, $H_{pyrrole}$), 8.85 (d, 4H, J = 4.0 Hz, $H_{pyrrole}$), 8.22 (d, 4H, J = 8.0 Hz, H_{phenyl}), 7.78−7.71 (m, 10H, H_{phenyl}), 7.22 (s, 2H, $H_{substituted\ phenyl}$), 4.18 (s, 6H, $H_{para-methoxy}$), 3.99 (s, 6H, $H_{meta,methoxy}$), −2.75 (s, 2H, H_{NH}). IR (KBr pellet; ν/cm^{-1}): 3443 (br, −NH), 1510 (aromatic C═C), 1259 (−OCH_3), 797−703 (pyrrole, HC═C). The UV−vis spectral data and $E_{1/2}$ values are presented in Table 1.

III.B.2. Method 2. In this method, the procedure that was adopted was the same as that mentioned in method 1 for the synthesis of Me_2L_1, except the molar ratio for benzaldehyde (5.07 mL, 100 mM), 3,4-dimethoxybenzaldehyde (8.3 g, 100 mM), and pyrrole (7.0 mL, 100mM) used for the reaction was different. During the chromatographic separation, a third fraction was collected. This fraction was found to be the mixture of the cis {5,10-(bisphenyl)-15,20-[bis-(3,4-dimethoxy)]-21H,23H-porphyrin} and desired trans {5,15-(bisphenyl)-10,20-[bis-(3,4-dimethoxy)]-21H,23H-porphyrin} forms. This mixture was further purified by column chromatography, using a silica gel column (column dimensions: length 75 cm and diameter 4 cm) and $CHCl_3$/*n*-hexane (95:5 v/v) as the eluent to start with. The polarity of the eluent mixture was raised by slowly decreasing the proportion for *n*-hexane. Eventually, the desired trans derivative was eluted with pure $CHCl_3$. The yield of the pure product was 0.400 g (∼2.2%). The R_f value and other analytical data for this were found to be similar to those for Me_4L_3 obtained by following method 1.

III.C. H_4L_3. The procedure adopted for the demethylation of Me_4L_3 (0.250 g, 0.341 mM) was similar to the one adopted for Me_2L_1. The yield for H_4L_3 was about 67% (0.155 g). Elem Anal. Calcd: C, 77.87; H, 4.42; N, 8.25. Found: C, 77.2; H, 4.6; N, 8.1%. FAB−MS: 678 (M^+). ^{1}H NMR ($CDCl_3$, ppm): δ_H 8.95 (d, 4H, J = 4.4 Hz, $H_{pyrrole}$), 8.84 (d, 4H, J = 4.4 Hz, $H_{pyrrole}$), 8.27−8.22 (m, 4H, H_{phenyl}), 7.85−7.75 (m, 8H, H_{phenyl}), 7.57 (d, 2H, J = 8 Hz, $H_{substituted\ phenyl}$), 7.29 (s, 2H, $H_{substituted\ phenyl}$), −2.75 (s, 2H, H_{NH}). IR (KBr pellet; ν/cm^{-1}): 3396 (br, −NH and −OH), 1272 (C−O), 798 (pyrrole C═C). The UV−vis spectral data and $E_{1/2}$ values are summarized in Table 1.

III.D. Me_2L_2. A total of 0.150 g (0.222 mM) of Me_2L_1 was dissolved in ∼80 mL of N,N-dimethylformamide in a round-bottom flask and heated to reflux. Then, an excess of $Zn(CH_3COO)_2 \cdot 2H_2O$ (0.200 g, 0.90 mM) was added to that mixture in three parts in 15−20 min intervals. The color of the solution changed from purple to deep blue-green. The mixture was allowed to reflux for 1 h, and then, it was cooled to room temperature. The reaction mixture was poured into ∼300 mL of ice-cold distilled water and kept refrigerated overnight. The precipitates obtained were filtered off, washed twice with water, and then dried in air. The precipitates were redissolved in a minimum amount of $CHCl_3$ and, then, subjected to column chromatography, using silica gel as the stationary phase and a $CHCl_3$/methanol (95:5 v/v) mixture as the eluent. The first major deep-purple band was found to be the desired product. Yield: 0.130 g (90%). The isolated product was characterized by various analytical and spectroscopic techniques. Elem Anal. Calcd: C, 74.85; H, 4.37; N, 7.59. Found: C, 74.3; H, 4.2; N, 7.2. FAB−MS: 737 (M^+). ^{1}H NMR ($CDCl_3$, ppm): δ_H 9.02−8.93 (m, 8H, $H_{pyrrole}$), 8.2 (d, 6H, J = 8.0 Hz, H_{phenyl}), 7.76−7.48 (m, 11H, H_{phenyl}), 7.23 (d, 1H, J = 8.0 Hz, $H_{substituted\ phenyl}$), 4.09 (s, 3H, $H_{para\ methoxy}$), 3.90 (s, 3H, $H_{meta\ methoxy}$). IR (KBr pellet; ν/cm^{-1}): 1026 (−OCH_3), 997 (C−O), 796 (pyrrole, C═C). The UV−vis spectral data and $E_{1/2}$ values are given in Table 1.

III.E. H_2L_2. This metalated porphyrin was synthesized following a synthetic methodology similar to that adopted for Me_2L_2. The only exception is that 1.4 equiv (0.116 g, 0.52 mM) of $Zn(CH_3COO)_2 \cdot 2H_2O$ was used for the reaction with 0.243 g (0.37 mM) of H_2L_1. Yield: 0.244 g (93%). Elem Anal. Calcd: C, 74.44; H, 3.95; N, 7.89. Found: C, 73.9; H, 4.1; N, 7.8. FAB−MS: 709 (M^+). ^{1}H NMR (CD_2Cl_2, ppm): δ_H 9.03−9.01 (2H, $H_{pyrrole}$), 8.94−8.92 (m, 6H, $H_{pyrrole}$), 8.21 (d, 6H, J = 7.4 Hz, H_{phenyl}), 7.78−7.53 (m, 11H, H_{phenyl}), 7.22 (d, 1H, J = 8.0 Hz, $H_{substituted\ phenyl}$). IR (KBr pellet; ν/cm^{-1}): 3428 (br, −OH), 995 (C−O), 795 (pyrrole, C═C). The UV−vis spectral data and $E_{1/2}$ values are given in Table 1.

III.F. Me_4L_4. This was synthesized by reacting $Zn(CH_3COO)_2 \cdot 2H_2O$ (0.062 g, 0.28 mM) and Me_4L_3 (0.070 g, 0.095 mM), following the same procedure as that adopted for the preparation of Me_2L_2. Yield: 0.130 g (90%). Elem Anal. Calcd: C, 72.23; H, 4.55; N, 7.02. Found: C, 71.6; H, 4.5; N, 6.8%. FAB−MS: 797 (M^+). ^{1}H NMR ($CDCl_3$, ppm): δ_H 9.02−9.0 (4H, J = 4.8 Hz, $H_{pyrrole}$), 8.96−8.94 (4H, J = 4.6 Hz, $H_{pyrrole}$), 8.22 (d, 4H, J = 8.0 Hz, $H_{phenyl\ ring}$), 7.79−7.76 (m, 10H, $H_{phenyl\ ring}$), 7.26 (d, 2H, J = 8.0 Hz, $H_{substituted\ phenyl}$), 4.18 (s, 6H, $H_{para\ methoxy}$), 3.98 (s, 6H, $H_{meta\ methoxy}$). IR (KBr pellet; ν/cm^{-1}): 1027 (−OCH_3), 1001 (C−O), 797 (pyrrole, C═C). The UV−vis spectral data and $E_{1/2}$ values are presented in Table 1.

III.G. H_4L_4. This compound was synthesized following the above-mentioned procedure, resulting in a yield of ∼85%, by reacting H_4L_3 (0.068 g, 0.100 mM) and $Zn(CH_3COO)_2 \cdot 2H_2O$ (0.045 g, 0.2 mM). However, this crude product could not be purified using column chromatography because of its limited solubility in common organic solvents. The crude product was washed thoroughly with $CHCl_3$ to remove any unreacted H_4L_3 and was used as such for further reactions. Yield: 85% (0.060 g). Elem Anal. Calcd: C, 71.21; H, 3.77; N, 7.55. Found: C, 70.8; H, 4.0; N, 7.4. FAB−MS: 741 (M^+). IR (KBr pellet; ν/cm^{-1}): 3429 (br, −OH), 995 (C−O), 797 (pyrrole, C═C). The UV−vis and redox potential values are provided in Table 1.

III.H. Complex 1. To an ethanolic solution of ligand H_2L_1 (0.300 g, 0.464 mM) was added ∼2.1 equiv of KOH (0.054 g), and the reaction mixture was allowed to warm to ∼60 °C under an argon atmosphere. Then, $Ru(bpy)_2Cl_2 \cdot 2H_2O$ (0.248 g, 0.48 mM) was added to it. The resulting mixture was refluxed for 5 h in an inert atmosphere and was allowed to cool to room temperature. $FcPF_6$ (0.154 g, 0.046 mM) was added to this, and the mixture was left exposed to the air with stirring at room temperature for 30 min. After that, an excess aqueous solution of KPF_6 was added, and the volume was reduced in vacuo to give a dark-brown precipitate. This was filtered off, washed with cold water, diethyl ether, and air dried. Column chromatography with a 100−200 mesh-size silica column and CH_3CN/aq·NH_4PF_6 (98:2 v/v) as the eluent gave the desired product as the first major band. This was dried under reduced pressure and redissolved in CH_2Cl_2, and excess hexfluoro-

Table 2. Electronic Spectral Data and Redox Potential Values for Complexes **1**−**4**

complex	λ_{max} ($\epsilon \times 10^4$ dm^3 mol^{-1} cm^{-1})[a]	porphyrin-/bpy-based $E_{1/2}$ (ΔE mV)[b]	dioxolene based $E_{1/2}$ (ΔE mV)[b] sq/cat	dioxolene based sq/q	$E_{1/2}$ (ΔE mV)[b] $Ru^{II/III}$
1	292 (34), 419 (229), 515 (15.2), 549 (7.8), 588 (5.4), 927 (6.4)	0.46 (110), 0.78 (120), −1.79 (140), −2.17 (145)	−0.68 (75)	0.227 (80)	1.07 (140)
2	291 (51.1), 419 (276), 546 (18.1), 584 (4.5), 933 (8.5)	0.45 (80), 0.71 (90), −1.82 (120), −2.19 (150)	−0.66 (80)	0.14 (70)	1.05 (100)
$[2]_{red}$	420 (364), 546 (45.2)				
$[2]_{ox}$	415 (308), 547 (35.1)				
3	286 (107), 418 (298), 514 (17), 548 (9.1), 910 (79.2)	0.4 (110), 0.74 (80), 1.1 (100), −1.89 (120), −2.14 (140)	−0.66 (120)	0.14 (125)	1.02 (140)
4	286 (142), 420 (302), 545 (18.2), 945 (83.5)	0.46 (110), 0.8 (85), −1.67 (110), −2.0 (115), −2.29 (125)	−0.66 (120)	0.30 (135)	1.06 (126)
$[4]_{red}$	424 (333), 555 (61.3)				
$[4]_{ox}$	408 (289), 558 (43)				

[a] Electronic spectra were recorded in CH_2Cl_2. Spectra of the electroreduced and -oxidized species were recorded in situ in the presence of 0.1 M $[Bu^t]N_4PF_6$ in CH_3CN. [b] Cyclic voltammograms were recorded in CH_3CN in 0.1 M $[Bu^t]_4NPF_6$. The potential values are reported (scan rate of 100 mVs^{-1}) versus those of the ferrocene/ferrocenium couple. Electrochemical measurements were made with Pt bead as the working electrode, Pt wire as an auxiliary electrode, and Ag−AgCl as the reference electrode.

phosphate salt was removed in the aqueous layer by solvent extraction. The CH_2Cl_2 layer was dried, and the compound thus obtained was further purified by additional gravity chromatography, using grade III Al_2O_3 as the stationary phase and a freshly distilled CH_3CN/toluene (7:3 v/v) solvent mixture as the eluent. The first major fraction was found to contain the pure desired product. Yield: 0.390 g (∼70%). Elem Anal. Calcd: C, 63.84; H, 3.66; N, 9.31. Found: C, 62.9; H, 3.9; N, 8.9. FAB−MS: 1202 (M^+, ∼2%), 1057 (M^+-PF_6, 25%). IR (KBr pellet; ν/cm^{-1}): 1443 (semi-quinone stretching), 841 (PF_6). EPR spectral data (77 K; CH_2Cl_2-toluene glass): g^1, 2.058; g^2, 1.9885; g^3,1.9585; g_{av}, 2.0016. The UV−vis/NIR spectral data and redox potential values are presented in Table 2.

III.I. $\{(bpy)_2Ru(H_2L_3)\}_{sq}[PF_6]$ (H_2L_3 is the doubly deprotonated form of H_4L_3). The synthetic procedure for this compound is similar to that of complex **1**, except H_4L_3 was used as the catechol derivative. H_4L_3 (0.28 g, 0.412 mM), KOH (0.047 g, 0.84 mM), and $Ru(bpy)_2Cl_2\cdot 2H_2O$ (0.214g, 0.412 mM) were used for the reaction. Yield: 0.345 g (∼65%). FAB−MS: 1090 (M^+, <10%), 945 (M^+-PF_6, ∼20%). IR (KBr pellet; ν/cm^{-1}): 1447 (semi-quinone stretching), 840 (PF_6).

III.J. Complex 2. The synthetic methodology followed for this complex is similar to that for complex **1**, except H_2L_2 (0.100 g, 0.141 mM), KOH (0.016 g, 0.29 mM), and $Ru(bpy)_2Cl_2\cdot 2H_2O$ (0.074 g, 0.14 mM) were used for the reaction. Yield: 0.130 g (∼72%). This was characterized by standard analytical and spectroscopic techniques. Elem Anal. Calcd: C, 60.65; H, 3.42; N, 8.85. Found: C, 60.4; H, 3.4; N, 8.6. FAB−MS: 1120 (M^+-PF_6, 10%). IR (KBr pellet; ν/cm^{-1}): 1443 (semi-quinone stretching), 841 (PF_6). EPR spectral data (77 K; CH_2Cl_2−toluene glass): g^1, 2.058; g^2, 1.99; g^3, 1.958; g_{av}, 2.0015. The UV−vis/NIR spectral data and redox potential values are provided in Table 2.

III.K.1. Complex 3. Method 1. This synthetic procedure is similar to that for complex **1**, except H_4L_3 was used as the ligand. H_4L_3 (0.300 g, 0.442 mM), KOH (0.105 g, 1.2 mM), and $Ru(bpy)_2Cl_2\cdot 2H_2O$ (0.336 g, 0.647 mM) were used for the reaction. During chromatographic purification, the desired product was eluted as the first fraction. Yield: 0.26 g (50%). Elem Anal. Calcd: C, 56.31; H, 3.24; N, 9.39. Found: C, 56.0; H, 3.2; N, 9.2. FAB−MS: 1789 (M^+, ∼2%): 1644 (M^+-PF_6, ∼15%). IR (KBr pellet; ν/cm^{-1}): 1447 (semi-quinone stretching), 840 (PF_6). EPR spectral data (77 K; CH_2Cl_2−toluene glass): g^1, 2.0593; g^2, 1.9965; g^3, 1.945; g_{av}, 2.001. The UV−vis/NIR spectral data and redox potential values are presented in Table 2.

III.K.2. Method 2. This synthetic procedure is similar to that adopted for complex **1**. A total of 0.124 g (0.1 mM) of $\{(bpy)_2Ru(H_2L_3)\}_{sq}[PF_6]$, dissolved in ethanolic KOH (0.012g, 0.21 mM), was reacted with 0.057 g (0.11 mM) of $Ru(bpy)_2Cl_2\cdot 2H_2O$. Yield: 0.143 g (80%). The purification procedure is similar to that followed for method 1. The analytical and various spectroscopic data are similar to those of the desired product synthesized following method 1.

III.L.1. Complex 4. Method 1. Complex **3** (0.110 g, 0.061 mM) was dissolved in 50 mL of CH_3OH and allowed to warm to ∼60 °C; to this, $Zn(CH_3COO)_2\cdot 2H_2O$ (0.054 g, 0.246 mM) was added, and the resulting mixture was refluxed for 1.5 h under an argon atmosphere. Then, the solution was dried in vacuo. The solid residue was redissolved in a minimum amount of CH_3CN and purified by column chromatography on a silica column (100−200 mesh size), using a CH_3CN/aq·NH_4PF_6 (98:2 v/v) mixture as eluent. The first major fraction was found to be the desired product and was collected. This was dried in vacuo and redissolved in CH_2Cl_2; excess NH_4PF_6 was removed in the aqueous layer through solvent extraction. Yield: 0.082 g (71%). Elem Anal. Calcd: C, 54.38; H, 3.02; N, 9.06. Found: C, 54.3; H, 3.3; N, 9.0. FAB−MS: 1708 (M^+-PF_6, ∼25%). IR (KBr pellet; ν/cm^{-1}): 1447 (semi-quinone stretching), 840 (PF_6). EPR spectral data (77 K; CH_2Cl_2−toluene glass): g^1, 2.0596; g^2, 1.998; g^3, 1.949; g_{av}, 2.0011. Various spectroscopic data and redox potential values are summarized in Table 2.

III.L.2. Method 2. This synthetic procedure is similar to that adopted in method 1 for complex **3**, except H_4L_4 was used as the ligand instead of H_4L_3. H_4L_4 (0.125 g, 0.168 mM), KOH (0.017 g, 2.1 mM), and $Ru(bpy)_2Cl_2\cdot 2H_2O$ (0.175 g, 0.336 mM) were used for the reaction. Yield: 0.195 g (∼65%). Analytical and spectroscopic data and redox potential values are similar to those observed for complex **4** synthesized following method 1.

Results and Discussion

Ligand 5-(3,4-dimethoxyphenyl)-10,15,20-triphenyl-21H, 23H-porphyrin (Me_2L_1) was prepared following the standard "one-pot synthesis" procedure, resulting in a reasonable yield. Attempts to improve the yield for Me_2L_1 by repeating the reaction in CH_2Cl_2 in the presence of a catalytic amount of TFA were not successful. The selective synthesis of trans bis-substituted porphyrin, 5,15-bis(3,4-dimethoxyphenyl)-10,20-bisphenyl-21H,23H-porphyrin (Me_4L_3), was prepared

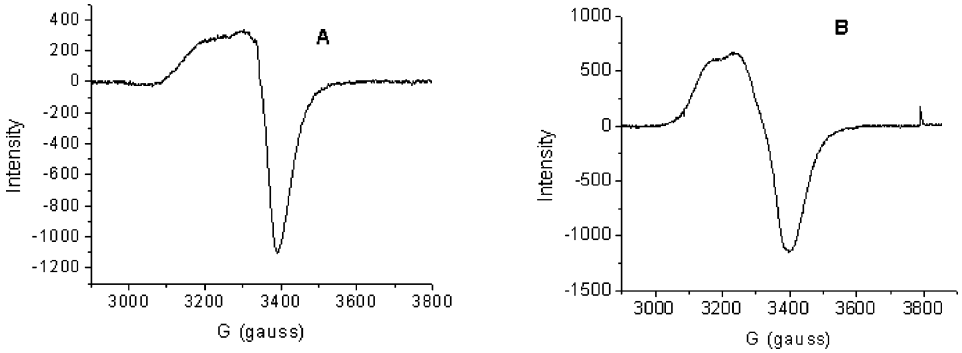

Figure 1. EPR spectra recorded for **1** (A) and **3** (B) at 77 K in CH_2Cl_2/toluene glass.

by employing a building block approach[23] through the condensation of presynthesized *meso*-phenyldipyrromethane with 1 mol equiv of 3,4-dimethoxybenzaldehyde. This was followed by the oxidation of the intermediate product with *p*-chloranil. The demethylations of Me_2L_1 and Me_4L_3 were achieved in molten pyrridinium hydrochloride salt at ∼160−165 °C in an inert atmosphere. An increase in the reaction temperature to ∼170−180 °C resulted in the desired porphyrin derivative with a considerably lower yield (<50%). Attempts to achieve a better yield for the demethylation reaction in a CH_2Cl_2 solvent and with BBr_3 as a catalyst, following standard procedure,[24] were not successful either (yield < 35%). These free-base porphyrin ligands are metalated with Zn^{II} following standard procedures. Ruthenium−dioxolene complexes, **1**−**4**, are synthesized from reactions of the completely deprotonated form of 5-(3,4-dihydroxyphenyl)-10,15,20-triphenyl-21H,23H-porphyrin (H_2L_1), 5,10-bis(3,4-dihydroxyphenyl)-10,20-bisphenyl-21H,23H-porphyrin (H_4L_3), the corresponding Zn derivatives (H_2L_2 and H_4L_4, respectively), and an appropriate mol equiv of $Ru(bpy)_2Cl_2 \cdot 2H_2O$ in absolute ethanol. After refluxing for 4 h, the reaction mixture was cooled and exposed to the air to ensure the oxidation of the initially formed catecholate complex to the corresponding semi-quinone form. Part of the oxidative conversion from the $Ru(bpy)_2$(cat*) fragment to the $Ru(bpy)_2(sq)^+$ fragment (cat* is a substituted catechol derivative) may also take place during the workup procedure or during column chromatography as the complexes get exposure to the air. SiO_2 and Al_2O_3, used as column material, are also known to act as the oxidant.[25] In a few cases, to avoid any possibility of an incomplete conversion to the semi-quinone form, a mild oxidant ($FcPF_6$) was added to the crude reaction mixture at room temperature. Analytical data (elemental analysis and electrospray mass spectral data) and the results of the various spectroscopic data [viz., vibrational; electronic; ^1H NMR spectral data for Me_2L_1, H_2L_1, H_2L_2, Me_4L_3, H_4L_3, and H_4L_4; and electron spin resonance (ESR) spectra data for **1**, **2**, **3**, and **4**] agree well with the formulations proposed for the respective ligands and the corresponding complexes.

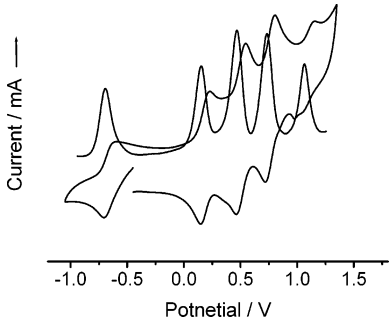

Figure 2. Cyclic voltammogram (200 mVs^{-1}) and differential-pulse voltammetry of **2** in CH_3CN. The potential scale shown is for the Fc/Fc^+ couple.

Complexes **1**−**4** were found to be paramagnetic and ESR-active. The paramagnetic nature of these dioxolene derivatives excludes the possibility of these complexes being present as either catecholate or quinone derivatives.[4,9−11] These complexes show a featureless room-temperature ESR spectrum consisting of a broadened signal centered at $g_{av} \approx 2.003$ in CH_2Cl_2. However, spectra recorded at 77 K are anisotropic (Figure 1) because the molecular orbital containing the unpaired electrons of the semi-quinone fragments is partially localized on the ruthenium center.[4,9−11] The room-temperature spectral features of the mono- (complexes **1** and **2**) and biradical (complexes **3** and **4**) species are similar, except that the spectra for monoradical species are less broad than those for biradical ones, presumably because of a weak interaction between the unpaired electrons of the two semi-quinone fragments.

A weak electronic interaction between the two redox-active $Ru(bpy)_2(sq)^+$ fragments is also evident in the results of cyclic and square wave voltammetric studies for complexes **1**−**4** (Table 2). The porphyrin ligands and their Zn derivatives showed characteristic features because the porphyrin-based oxidation couple was observed within 0.6−0.8 V versus that of Fc/Fc^+, while the porphyrin-based reduction couple was observed within −1.5 to −1.85 V versus that of Fc/Fc^+. As expected, 3,4-dimethoxybenzene or 3,4-dihydroxybenzene fragments attached to the porphyrin ring and showed either quasi-reversible or irreversible dioxolene-based redox processes (Table 1).[11] For complexes **1**−**4**, the $Ru(bpy)_2(sq)$ cores undergo reversible redox processes at potentials consistent with that of the individual component along with the expected redox processes associated with the porphyrin core (Table 2). The representative cyclic voltam-

(23) (a) Lee, C.-H.; Lindsey, J. S. *Tetrahedron* **1994**, *50*, 11427. (b) Manka, J. S.; Lawrence, D. S. *Tetrahedron Lett.* **1989**, *30*, 6989.
(24) McOmie, J. F.; Watts, M. L.; West, E. *Tetrahedron* **1968**, *24*, 2289.
(25) Ernst, S.; Hanel, P.; Jordanov, J.; Kaim, W.; Kasack, V.; Roth, E. *J. Am Chem. Soc.* **1989**, *111*, 1733.

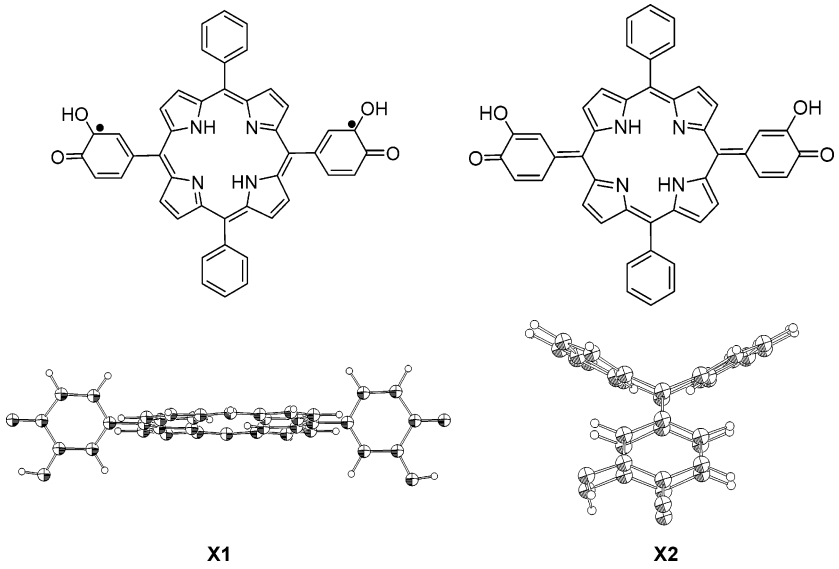

Figure 3. UPM3 optimized structures of model systems **X1** and **X2**.

mogram for complex **2** is shown in Figure 2. However, the cat/sq and sq/q redox waves for **3** and **4** are much broader [($E_{pc} - E_{pa}$) ≥ 120−135 mV; Table 2) than those observed for complexes **1** and **2**, which is understandable if one considers the possibility of overlapping redox waves for the two weakly interacting $Ru(bpy)_2(sq)^+$ fragments in **3** and **4**. Such behavior is not surprising if one considers that two appended ruthenium−semiquinone fragments are separated by ∼14.2 Å with an orthogonal orientation, with respect to the porphyrin plane (an analogous model system is represented as **X1**, vide infra).[20,21]

To corroborate the presumption, we have employed UHF PM3 calculations to optimize the geometry of two possible isomeric model compounds, **X1** and **X2**, at the UPM3 level (Figure 3).[21,22] The possibility of **X1** being present as biradical (singlet and triplet) has been considered. The energy-optimized geometry for model system **X1** (singlet and triplet) predicts a planar porphyrin ring and orthogonal sq-fragment orientations, with π electron delocalization in the porphyrin unit (Figure 3), while the planar orientation of the semi-quinone ring in **X2** causes the porphyrin ring to be away from a planar structure, with disruption of the π electron delocalization. The triplet form of the biradical **X1** is more stable than **X2** by 18.7 kcal/mol. Calculations also predict that the singlet form of biradical **X1** is less stable than the triplet form by 1.9 kcal/mol. Thus, the energy-minimized structure of the biradical species (**X1**) suggests an orthogonal orientation of the semi-quinone fragment with respect to the porphyrin plane in complexes **1**−**4** and thereby negates the possibility of extended conjugation and the delocalization of unpaired electrons across the bridging porphyrin core in complexes **2** and **4**.

Electronic spectral data for the ruthenium−dioxolene complexes along with those of the reduced and oxidized forms of **2** and **4** are presented in Table 2. Electronic spectral data reveal that bi-/trichromophoric systems, **1**−**4**, show expected spectral features of the individual mononuclear components along with an unusually strong absorbance at ∼940 nm for the $d\pi_{Ru} \rightarrow \pi^*_{bsq}$ transition (ϵ = 59 000−83 500 $dm^3mol^{-1}cm^{-1}$). To the best of our knowledge, barring two examples available in the literature to date,[1d,5] where the ϵ values reported for the absorption band in the NIR region are ∼100 000 $dm^3mol^{-1}cm^{-1}$, the ϵ values for the NIR absorption band observed for these complexes are among the highest known for any inorganic metal complexes. A red shift of ∼50 nm for λ_{max} of the MLCT ($d\pi_{Ru} \rightarrow \pi^*_{bsq}$) transition band of complexes **1**−**4**, compared to that for $Ru(bpy)_2(bsq)^+$ species),[8] is observed. An even higher red shift of ∼100 nm was observed by us for this MLCT band, where the coordinated sq functionality is part of an extended conjugated system.[11] Presumably, this higher red shift observed in the Ru^{II}−dioxolene complexes reported earlier is due to the more effective lowering of the energy of semiquinone singly occupied molecular orbitals arising from the extended conjugation.[8,9,11] This also indicates either the absence of any or the presence of little extended conjugation in complexes **1**−**4** and agrees well with the proposed conformation. A similar shift of ∼75 nm is reported by Ward and co-workers for the bi-/trinuclear complexes, where two $Ru(bpy)_2(sq)$ units are linked by a $Ru(tpy)_2$ center (tpy is a 2,2′:6′,2”-terpyridyl derivative).[26] For complexes **1**−**4**, sq-porphyrin or sq-porphyrin-sq$Ru(bpy)_2$ is expected to be a better electron acceptor than the bsq alone, and this, presumably, is responsible for the observed red shift.

Spectroelectrochemical studies with complexes **1**−**4** show that either oxidation or reduction of the semi-quinone fragment causes a complete bleaching of the MLCT band in the NIR region (Figure 4). Spectral changes are found to be completely reversible, and a quantitative recovery of the MLCT band at the NIR region occurs upon the reversal of the redox processes. This observation is in agreement with the reversible nature of the dioxolene-based redox processes, which is observed in cyclic voltammograms for complexes

(26) Whittle, B; Everest, N. S.; Howard, C.; Ward, M. D. *Inorg Chem.* **1995**, *34*, 2025.

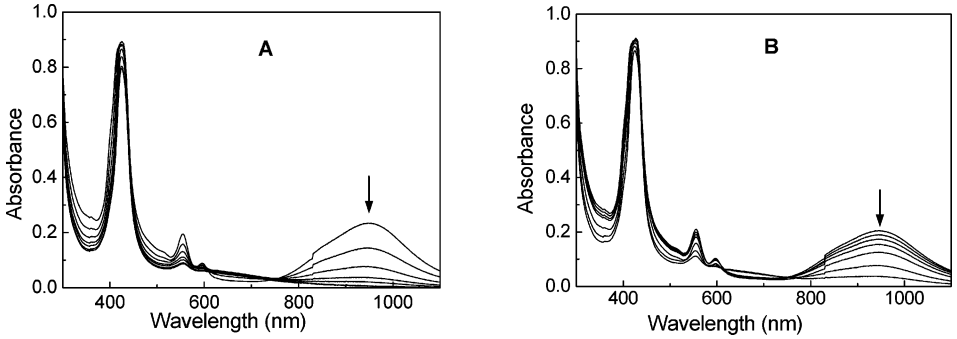

Figure 4. Electronic spectral changes when **4** is subjected to bulk electrolysis (A) −0.4 V (vs SCE) and (B) 0.7 V (vs SCE).

Table 3. Emission Data of Free-Base Porphyrine Derivatives and Their Dioxolene Complexes (**1**−**4**)[a]

compound	Q (0,0) λ_{max} (nm)	Q (0,1) λ_{max} (nm)	ϕ_f
H_2L_1	651 (239)	708 (16)	0.0977
H_4L_3	653 (275)	708 (17)	0.1117
complex **1**	652 (91)	707 (6.3)	0.03379
complex **3**	652 (23)		0.0093

	S_2 emission		S_1 emission		
compound	B (0,0) λ_{max} (nm)	$\phi_f \times 10^4$	Q (0,0) λ_{max} (nm)	Q (0,1) λ_{max} (nm)	ϕ_f
H_2L_2	436 (84)	1.37	596 (514)	640 (262)	0.03612
H_4L_4[b]					
complex **2**	433 (21)	0.32	595 (66)	640 (31)	0.0054
complex **4**	431 (37)	0.77	595 (35)	640 (15)	0.00393

[a] All of the spectra were recorded in CH_3CN. [b] Data could not be obtained because of its limited solubility in the desired solvent.

1−**4**. Thus, these complexes fulfill the basic criteria for possible use as redox switchable photochromic dyes.[27]

However, to understand the system better and to investigate the possibility of electron or energy transfer processes being involved, we looked into the steady-state emission properties of all the bi-/trichromophoric systems and the transient absorption spectra of the excited state of the simple bichromophoric system (**1**) and its individual mononuclear components on an ultrafast time scale. The data obtained from the steady-state emission measurements for the bichromophoric complexes of interest (**1**−**4**) reveal to us that the fluorescence quantum yield of the complex is at least 3 times less (Table 3) than that of the precursor molecule.

The emission lifetime measurements carried out for H_2L_1 and **1** have shown that there is no change in the emission lifetime of the porphyrin core in these two species when excited at 408 nm. The excited state lifetime for the porphyrin moiety was found to be 8.8 ± 0.2 ns. This suggests that the process that is responsible for the reduction in the fluorescence quantum yield is expected to be much faster than the time resolution of the time-correlated single photon counting (TCSPC) technique used for lifetime measurements (~200 ps). Thus, the observed decrement in the emission quantum yield may be due to intramolecular electrons or an energy transfer between $Ru(bpy)_2sq^+$ and porphyrin moieties, or it may occur through other nonradiative pathways. The quantum yield (ϕ) for the free ligand is ~0.1. On the basis of the definitions of ϕ [$\phi = k_r/(k_r + \sum k_{nr})$] and the lifetime [$\tau$; $\tau = 1/(k_r + \sum k_{nr})$], in terms of the radiative (k_r) rate constant and the sum of all of the nonradiative ($\sum k_{nr}$) rate constants, one may conclude that $\sum k_{nr} > k_r$. Therefore, if the value for ϕ has to decrease, either k_r should decrease or ($k_r + \sum k_{nr}$) must increase. However, if the latter were true, the value for τ would have decreased. In the present investigation, the observed value for τ is almost the same for both of the species (H_2L_1 and **1**). $\sum k_{nr}$ being the dominant term in the expression for ϕ, it is difficult to see how an additional term in $\sum k_{nr}$ (that accounts for a new, fast nonradiative decay) could be the cause of the quantum yield decrease without any change in the lifetime as well. Thus, our data tends to suggest that the presence of the $Ru(bpy)_2(sq)^+$ fragment somehow reduces the value for k_r. Because $\tau^*/\tau = k_r$ and the τ values are the same, then the change in ϕ reflects a change in k_r. Because H_2L_1 and **1** are two different compounds, it is quite possible that their natural radiative lifetimes (τ^*) will be different. (This interpretation was suggested by one of the reviewers and is consistent with the observed results.)

The possibility of an intramolecular energy transfer process can be ruled out because the emission spectra of the porphyrin core and the absorption spectra of the $Ru(bpy)_2sq^+$ fragment do not overlap. However, the possibility of electron transfer from photoexcited porphyrin to the $Ru(bpy)_2sq^+$ moiety may not be ruled out because the process is also favored thermodynamically. The other factor, which may also cause the decrease in the fluorescence quantum yield, is basically a consequence of the aggregation of the porphyrin molecules.[28] This possibility of aggregate formation can be clarified with the aid of concentration-dependent optical absorption and emission measurements. These did not show any red shift in the absorption spectrum with respect to the Soret band, which is the signature of aggregate formation.[28] These measurements have unambiguously nullified the plausible involvement of aggregate formation for the decrease in the quantum yield. To elucidate the actual mechanism for the decrement in the emission quantum yield of the complex molecule, excited-state dynamics of H_2L_1 and **1** have been studied using transient absorption spectroscopy in shorter time scales.

(27) DeSilva, A.P.; Gunaratne, H. Q. N.; Gunnaugsson, T.; Huxley, A. J. M.; McCoy, C. P.; Rademacher, J. T.; Rice, T. E. *Chem. Rev.* **1997**, *97*, 1515 and references therein.

(28) Akins, D. L.; Ozcelik, S.; Zhu, H.−Ru.; Guo, C. *J. Phys. Chem.* **1996**, *100*, 14390.

Table 4. Transient Decay Times of H_2L_1 and $[Ru(bpy)_2bsq]^+$ and Their Complex (**1**) at Representative Wavelengths Measured after Exciting with a 100 fs Laser Light at 400 nm

wavelength (nm)	H_2L_1/ACN τ in ps (a%)	**1**/ACN τ in ps (a%)	Ru−sq/ACN τ in ps (a%)
470	0.22 ± 0.05 (43.5)	0.28 ± 0.05 (32.3)	
	1.5 ± 0.2 (5.3)	1.5 ± 0.2 (24.7)	
	13 ± 2 (6.8)	10 ± 2 (3.1)	
	>400 (44.4)	>400 (39.9)	
550	0.22 ± 0.05 (33.8)	0.20 ± 0.05 (52.6)	
	1.4 ± 0.2 (16.2)	1.5 ± 0.2 (15.8)	
	10 ± 2 (8.1)	26 ± 2 (8.4)	
	>400 (41.9)	>400 (23.2)	
670	0.22 ± 0.05 (61.3)	0.23 ± 0.05 (72.2)	0.27 ± 0.05 (62.7)
	1.5 ± 0.2 (12.5)	1.4 ± 0.2 (8.3)	1.5 ± 0.2 (7.4)
	10 ± 2 (1.3)	28 ± 2 (8.2)	10 ± 2 (7.4)
	>400 (24.9)	>400 (11.3)	>400 (22.5)
710	0.20 ± 0.05 (51.1)	0.23 ± 0.05 (68.9)	
	1.5 ± 0.2 (17.8)	1.4 ± 0.2 (12.1)	
	13 ± 2 (12.9)	25 ± 2 (10.6)	
	>400 (18.2)	>400 (8.4%)	
900	0.21 ± 0.05 (50)	0.27 ± 0.05 (−83)	0.27 ± 0.05 (−65.7)
	1.5 ± 0.2 (10.3)	1.6 ± 0.2 (−12.3)	1.5 ± 0.2 (−15.7)
	10 ± 2 (3.1)	23 ± 3 (−8.9)	19 ± 3 (−22.4)
	>400 (46.6)	>400 (4.1)	>400 (3.8)

To understand the relaxation dynamics of the complex molecule **1**, it is crucial to study the excited-state dynamics of the porphyrin moiety separately. We have recorded transient absorption spectra for H_2L_1 in acetonitrile after exciting it with a 400 nm laser pulse (full width at half maximum = 100 fs), and we have shown them in Figure 5. The transient spectrum consists of absorption peaks centered at 490, 530, 570, 610, and 690 nm, with a dip at 510 nm. The observed transients for H_2L_1 are assigned to the S_1-S_n absorption bands. The dip at 510 nm is observed because of the overlapping ground-state absorption of the Q band of the porphyrin moiety. In addition, all of the sharp structures observed in the transient spectra correspond to the overlapping Q-band only. Kong and co-workers [30] have estimated the internal conversion rate ~ 10 fs from S_2 to S_1 for H_2TPP by the femtosecond time-resolved fluorescence depletion method, following excitation at 398 nm in chloroform. Similar ultrafast or instrument-limited increases of the S_1 state have also been observed by Zewail and co-workers[29] for H_2TPP, and experimental data of the fluorescence up-conversion measurements suggest that the time duration of internal conversion observed for the transition from the S_2 to S_1 state can be as fast as <50 fs for H_2TPP. Kinetic decay traces (after excitation by a 400 nm laser pulse) of the acetonitrile solution of H_2L_1 at 470 nm, 550 nm, and 710 nm, measured with femtosecond pump−probe spectroscopy, were obtained. Observed decay traces, at these respective wavelengths, can be best fitted with a multiexponential function with typical time constants of 300 fs, 2 ps, and 13 ps and a very long lifetime component for all of the wavelengths (Table 4). Zewail and co-workers[29] also had a similar observation while carrying out transient absorption measurements for H_2TPP, following excitation with a 397 nm femtosecond laser pulse; the transient absorption kinetics at 657 nm can be fitted multiexponentially with time constants of 200 fs, 1.4 ps, and 10−20 ps and a very long lifetime component. They have attributed three fast components, 200 fs, 1.4 ps, and 10−20 ps, to intramolecular vibrational energy redistribution, vibrational redistribution caused by elastic collision with solvent molecules, and thermal equilibration by energy exchange with the solvent, respectively. Similarly, we have also attributed the 300 fs component to intramolecular vibrational energy redistribution, the 2 ps component to vibration cooling, and the 13 ps component to thermal equilibration with the solvent. To understand and find out the decay time constant of the longer component, which is the excited-state lifetime of H_2L_1, we have measured the fluorescence lifetime using TCSPC measurements, and it has been found to be 8.8 ± 0.2 ns.

The transient absorption spectrum of **1** at various time delays, after excitation at 400 nm, is shown in Figure 6. The transient spectrum at each time delay consists of positive absorption peaks centered on 490, 550, 610, and 710 nm

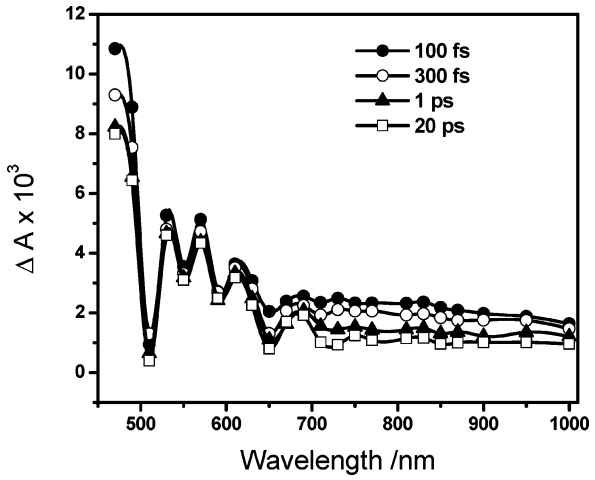

Figure 5. Transient absorption spectra of H_2L_1 in acetonitrile at different delay times after excitation at 400 nm. The transient absorption has been attributed to the S_1-S_n absorption.

(29) Baskin, J. S.; Yu, H. Z.; Zewail, A. H. *J. Phys. Chem. A* **2002**, *106*, 9837.
(30) Zhong, Q.; Wang, Z.; Liu, Y.; Zhu, Q. H.; Kong, F. A. *J. Chem. Phys.* **1996**, *105*, 5377.

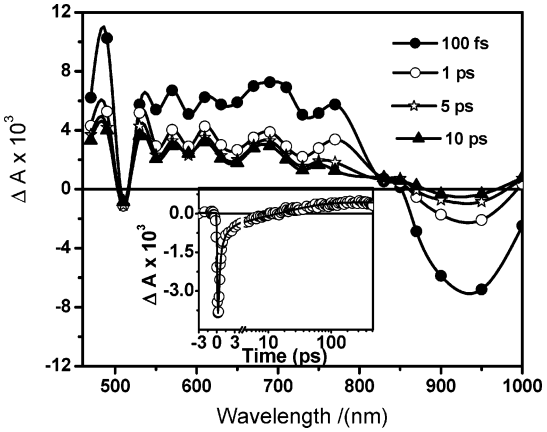

Figure 6. Transient absorption spectra of **1** in acetonitrile at different delay times after excitation at 400 nm. (The inset shows the bleach recovery kinetics monitored at 950 nm.)

along with a dip at 510 nm and strong bleaching in the 935 nm region. The positions of the transient absorption peaks matched pretty well with those of the transients in H_2L_1 (Figure 5). It is worth mentioning here that, even though the peak positions are similar, the relative intensities and width of the bands are markedly different. This is due to the fact that complex **1** is basically a different molecule, with the $Ru(bpy)_2(sq)$ fragment attached to the porphyrin moiety, compared to the individual fragment H_2L_1; the attached $Ru(bpy)_2(sq)$ fragment is expected to have an influence on the ϵ values of different bands. The additional big bleaching at 950 nm can be attributed to the disappearance of the absorption peak due to the $d\pi_{Ru} \rightarrow \pi^*_{sq}$-based MLCT transition of the $Ru(bpy)_2sq$ moiety of **1**. The dynamics of **1** have been monitored at various wavelengths (e.g., at 470 550, 670, and 710 nm), and the respective decay trace has been fitted with a multiexponential function with different time constants; these data are given in Table 4. It is interesting to note that the decay kinetics at 470 nm for **1** matched pretty well with those for H_2L_1 at the same wavelength and can be attributed to the excited-state dynamics of the photoexcited porphyrin moiety of **1** (vide infra). However, the decay kinetics for **1** at 670 and 710 nm are relatively faster than those observed for H_2L_1 at these respective wavelengths. We have also monitored bleaching recovery kinetics at 950 nm (inset of Figure 6), and they have also been fitted to a multiexponential function; the time constants that were obtained are provided in Table 4. In our earlier studies,[14c] we carried out a time-resolved transient absorption of **1** in acetonitrile following excitation at 532 nm with a picosecond laser pulse (full width at half maximum = 35 ps). We observed bleaching around 900 nm in the time-resolved spectra, which was attributed to the forward electron transfer from photoexcited porphyrin to the $Ru(bpy)_2sq$ moiety, while the recovery kinetics of the bleaching were attributed to the corresponding back electron-transfer process. Thus, our present in-depth study seems to contradict our earlier proposition based on experiments on a picosecond time domain. To resolve this further, we have also studied the excited-state dynamics of $[Ru(bpy)_2bsq]^+$ separately, after excitation at 400 nm.

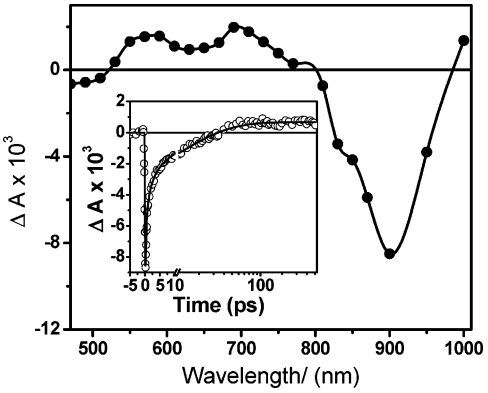

Figure 7. Transient absorption spectrum of $Ru(bpy)_2(bsq)^+$ in acetonitrile at a 100 fs time delay after excitation with a 400 nm laser pulse. The transient absorptions at 690 and 570 nm have been attributed to the excited- and triplet-state absorptions of $Ru(bpy)_2(bsq)^+$, respectively, and the negative absorption at 900 nm is due to the bleach of the ground-state absorption. (The inset shows the bleach recovery kinetics monitored at 900 nm.)

The transient absorption spectrum of photoexcited $[Ru(bpy)_2bsq]^+$ following excitation at 400 nm is shown in Figure 7. The transient spectrum consists of absorption peaks at 580 and 690 nm with a bleach at 900 nm; a similar bleach was observed for complex **1** and has been described earlier. The transient decay kinetics of the absorption have been fitted multiexponentially, and the respective rate constants are provided in Table 4. The transient peaks have been attributed to the excited-state absorption of the $d\pi_{Ru} \rightarrow \pi^*_{bsq}$-based MLCT transition of the $Ru(bpy)_2(bsq)^+$ moiety. The bleach at 900 nm (inset of Figure 7) can be attributed to the electron transfer from the photoexcited Ru^{II} center to the semi-quinone radical, while the recovery kinetics can be attributed to the back electron transfer from the reduced semi-quinone radical to the Ru^{III} center. Spectroelectrochemical studies on **1** and $[Ru(bpy)_2(bsq)]^+$ [11b] have already established that, for both complexes, the NIR absorption bands around 930 and 890 nm, respectively, bleach reversibly upon the reduction of the semi-quinone fragment to the corresponding catechol one and reappear with their original intensity upon the reversal of the redox process. As we have observed, in the present investigation, both porphyrin and $Ru(bpy)_2bsq$ moieties can be excited by a 400 nm laser pulse. Thus, it is expected that, in **1**, both porphyrin and $Ru(bpy)_2(sq)$ centers will get excited when they are exposed to a 400 nm laser pulse. One can expect that the transient absorption spectrum of **1** will be a mixture of the excited states of both porphyrin and $Ru(bpy)_2sq$ fragments, unless there is any interaction between them in the excited states. Although, Figure 6 shows that the transient spectrum for **1** is roughly an addition of the transient spectra of two individual components, H_2L_1 (Figure 5) and $Ru(bpy)_2bsq^+$ (Figure 7); slight variation is observed as a result of the differences in the energy and ϵ values associated with the MLCT transition for the $d\pi_{Ru} \rightarrow \pi^*_{sq}$-based transitions in **1** and $Ru(bpy)_2(bsq)^+$. Further, in the transient spectrum of **1**, we have observed neither any special transient due to the porphyrin cation radical nor any transient growth in the absorption spectrum in the wavelength region studied (460−1000 nm; Figure 6) when it was excited at 400 nm. Thus, we can unambiguously rule out the possibility of electron

transfer from the photoexcited porphyrin moiety to the $Ru(bpy)_2sq$ fragment. In the present investigation, the bleach at 950 nm is instantaneous, which is due to a direct photoexcitation of the $Ru(bpy)_2(sq)$ moiety instead of an excited energy transfer from the porphyrin moiety. Hence, we can rule out the possibility of an intramolecular energy transfer process within the photoexcited complex.

The above results suggest that the excited-state dynamics of **1** are a combination of the deactivations of the two individual moieties. Thus, the dynamics of the complex molecule, **1**, on photoexcitation is explained in the following manner. The fast component of 220 fs has been assigned to an intramolecular vibrational relaxation similar to that of H_2L_1; only, the amplitude of the decay is more in that of **1**. The 1.6 and 11 ps components can be assigned to the vibrational cooling. The long-lived transient is the singlet state of the molecule, which decays with a long lifetime.

In conclusion, the excited-state deactivation of the porphyrin center, linked with the $Ru(bpy)_2(sq)$ moiety, reveals that the observed dynamics are a mixed set, having independent contributions from the porphyrin and $Ru(bpy)_2(sq)$ components. The results unambiguously rule out the possibility of either an electron or energy transfer from the porphyrin to the $Ru(bpy)_2(sq)^+$ fragment or vice versa. The observed decrement in the luminescence quantum yield can be ascribed to the increased nonradiative pathway due to large vibronic coupling because of the direct linkage of the metal center to the porphyrin moiety.

Acknowledgment. The Department of Science and Technology (DST) and the Board of Research in Nuclear Science (BRNS), government of India, support this work. Authors D.A.J., A.D.S., and D.K.K. acknowledge CSIR for the Sr. Research Fellowship. We also thank all of the reviewers for their suggestions and comments. A.D. and H.N.G. acknowledge Dr. P. K. Ghosh (CSMCRI, Bhavnagar, India) and Dr. T. Mukherjee (BARC, Mumbai, India) for their keen interest in this work.

Supporting Information Available: Schemes for the redox processes involving $Ru(bpy)_2(bsq)^+$, synthetic methodologies for the syntheses of Me_2L_1 and H_4L_3, room-temperature EPR spectra for complexes **1** (A) and **3** (B), relative energy diagrams for **X1** (both singlet and triplet forms) and **X2**, and kinetic decay traces of the different transients of H_2L_1 and L_1 in acetonitrile monitored at different wavelengths. This material is available free of charge via the Internet at http://pubs.acs.org.

IC048805L